ARCHIVIO ISTITUZIONALE DELLA RICERCA

Alma Mater Studiorum Università di Bologna
Archivio istituzionale della ricerca

Novel Dual-Action Plant Fertilizer and Urease Inhibitor: Urea·Catechol Cocrystal. Characterization and Environmental Reactivity

This is the final peer-reviewed author's accepted manuscript (postprint) of the following publication:

*Published Version:*
Casali, L., Mazzei, L., Shemchuk, O., Sharma, L., Honer, K., Grepioni, F., et al. (2018). Novel Dual-Action Plant Fertilizer and Urease Inhibitor: Urea·Catechol Cocrystal. Characterization and Environmental Reactivity. ACS SUSTAINABLE CHEMISTRY & ENGINEERING, 7(2), 2852-2859 [10.1021/acssuschemeng.8b06293].

*Availability:*
This version is available at: https://hdl.handle.net/11585/708862 since: 2024-04-22

*Published:*

DOI: http://doi.org/10.1021/acssuschemeng.8b06293

*Terms of use:*

Some rights reserved. The terms and conditions for the reuse of this version of the manuscript are specified in the publishing policy. For all terms of use and more information see the publisher's website.

This item was downloaded from IRIS Università di Bologna (https://cris.unibo.it/).
When citing, please refer to the published version.

(Article begins on next page)

11 October 2026

# A novel dual-action plant fertilizer and urease inhibitor: the urea·catechol co-crystal - characterization and environmental reactivity

Lucia Casali,[a] Luca Mazzei,[b] Oleksii Shemchuk,[a] Lohit Sharma,[c] Kenneth Honer,[c] Fabrizia Grepioni,[a]* Stefano Ciurli,[b]* Dario Braga[a] and Jonas Baltrusaitis[c]*

a. Molecular Crystal Engineering Laboratory, Dipartimento di Chimica G. Ciamician, Università di Bologna Via F. Selmi, 2, 40126 Bologna, Italy

b. Laboratory of Bioinorganic Chemistry, Department of Pharmacy and Biotechnology, University of Bologna, Viale Giuseppe Fanin 40, 40127 Bologna, Italy

c. Department of Chemical and Biomolecular Engineering, Lehigh University, 111 Research drive, Bethlehem, PA 18015, USA

*Corresponding author: job314@lehigh.edu, fabrizia.grepioni@unibo.it, stefano.ciurli@unibo.it

## Abstract

Mechanochemical reaction of urea and catechol affords quantitative formation of a 1:1 urea·catechol co-crystal that can act simultaneously as a urease inhibitor and as a soil fertilizer. The novel compound has been characterized using solid state methods, and its environmental activity has been assessed using inhibition of *Canavalia ensiformis* urease and water vapor sorption experiments at room temperature. The urea molecules within the co-crystal were organized in hydrogen bonded dimers bridged by two catechol molecules, with the OH groups interacting via hydrogen bonds with the urea carbonyl groups. The inhibition of jack bean urease enzyme by URCAT led to the complete loss of urease activity after a 20-min incubation period. A large difference of water vapor adsorption was observed between urea and URCAT, with the latter adsorbing 3.5 times less water than urea. Our results suggested that co-crystal engineering strategies can be successfully applied to tackle sustainability problems at the food-energy-water nexus.

**Keywords:** nitrogen; urea; co-crystal; environment; nutrients

**Introduction.** Urea is a major nitrogen (N) containing soil fertilizer, synthesized from ammonia ($NH_3$) and carbon dioxide ($CO_2$), with an annual production projected to reach 226 million tons in 2021.[1] Once deposited in soil, urea quickly hydrolyzes in moist environment to yield $NH_4^+$ and $HCO_3^-$.[2] This reaction causes a number of agronomic,[3] environmental[4–6] and economic[7–9] problems[10] and affects the global N cycle.[11–13] In particular, too rapid increase of soil pH upon urea hydrolysis, catalyzed by urease activity,[14] causes the loss of urea nitrogen as gaseous $NH_3$. Ammonia is toxic to plants[15] contributes to the production of fine inorganic particulate matter ($PM_{2.5}$),[16] a well-documented factor for premature population mortality[17] as ammonium−sulfate−nitrate salts.[18] Furthermore, ammonia nitrification produces additional N loss due to nitrate leaching and/or denitrification, the latter causing tropospheric pollution by NO, $NO_2$ and especially $N_2O$, a greenhouse gas with 300 times the heat-trapping capacity of $CO_2$.[9,13] Exogenous inorganic and organic molecules are often introduced into soil with urea in order to inhibit urease activity, thus affecting urea chemistry.[19] Reversible inhibitors that target the Ni(II) ions in the active urease site can be utilized, such as phosphate, diamidophosphate, thiols, sulfite, fluoride, as well as hydroxamic, citric and boric acids, while Michael-type reagents such as catechols or quinones irreversibly target enzyme cysteine thiols essential for catalysis.[14,20–22] A widely used urease inhibitor is the organophosphorus compound N-(n-butyl)thiophosphoric triamide (NBPT), whose mechanism of action has been recently elucidated.[23] Considering that some negative effects of NBPT on living cells of plants[24,25] and microorganisms[26] have been reported, conceptually new methods to mitigate urea reactivity need to be developed. Within this framework an approach based on acidic polymers was shown to be effective.[27] Recent attempts to improve urea stability[28–31] in soil have exploited its excellent and well-established propensity to form molecular and ionic cocrystals.[32–35] In particular, two types of urea co-crystals have been

utilized to stabilize its reactivity towards hydrolysis and decrease concurrent emissions of ammonia.

First, urea physicochemical stabilization via encapsulation with ionic metal salts or the corresponding acids was utilized. Some field measurement evidence reveals that urea coordination compounds can reduce N losses from soils. For example, agricultural field tests with $NH_4Cl$ or $ZnSO_4$ have been shown to reduce $NH_3$ losses from soil and improve overall nitrogen uptake efficiency when *compacted* with urea.[36] Inhibition of urea reactivity by organic or inorganic acids, such as phosphoric acid, was shown to decrease $NH_3$ emissions up to 50 % from soil fertilized with urea phosphate ionic cocrystal.[37] Von Rheinbaben[38] and Fenn *et al.*[39] showed significant decrease of $NH_3$ emissions for applied or reactively formed urea·$Mg(Ca)SO_4$ (or presumably urea adducts with $CaCl_2$ and $Ca(NO_3)_2$ formed *in situ* in soil), but the reaction mechanisms put forth were inconclusive, as other authors showed that sulfate salts were not effective $NH_3$ emission regulators[40]. Very recently, green mechanochemical methods were applied to synthesize urea ionic co-crystals, including 4urea·$CaSO_4$·directly from salts[30] and using reactive mechanochemistry[31] with urea inorganic acid co-crystals.

Second, urea co-crystals with urease inhibiting metals or organic compounds have been utilized. Recently, it has been shown that metal ions acting as urease inhibitors, such as $Zn^{2+}$, can be associated within the same ionic co-crystal with plant nutrients, such as $K^+$, and with urea.[28] The co-crystal urea·$ZnCl_2$·KCl has been shown to effectively inhibit urease activity in a concentration-dependent manner. An old study on the inhibition of urease activity in soils showed that diphenols and quinones are particularly effective.[14] Recently, the kinetics of urease inhibition by benzoquinone, and the structure of the corresponding urease-inhibitor complex, have been elucidated.[41] Catechol (1,2-dihydroxy benzene) is another type of polyphenol that has been known

for several decades to inhibit soil urease,[14] but only recently its mode of action was elucidated through a combined kinetic and structural study.[42]

In this paper we report on the preparation, structural characterization and evaluation of the environmental activity of a novel double-action material based on the association of urea with catechol. The objective is providing, simultaneously, a potent urease inhibitor, catechol, together with a fundamental high N content fertilizer, such as urea.

## Experimental

**Reagents and solutions.** All reagents were purchased from Sigma-Aldrich or Alfa Aesar and used without further purification.

**Solution Synthesis.** Equimolar quantities of the starting materials (0.58 mmol) were dissolved in water or ethanol and left to evaporate at room temperature.

**Solid State Synthesis.** The co-crystal was obtained by ball-milling urea (1 mmol) with catechol (1 mmol) in an agate jar for 60 min in dry conditions or with the addition of a drop of water.

**Single crystal growth.** Single crystals suitable for X-ray diffraction were grown from an ethanol solution of the reagents in 1:1 stoichiometric ratio.

**Slurry experiments.** Slurry experiments were performed in water at room temperature for one week, to check for the possible formation of different solid forms. In all cases the urea·catechol co-crystal was recovered.

**Differential Scanning Calorimetry.** DSC traces were recorded using a Perkin-Elmer Diamond. The samples (1-3 mg range) were placed in open Al-pans. All measurements were conducted in

the ranges 40-150/160/170 °C (for urea, catechol and URECAT) at a heating rate of 5 ºC $min^{-1}$. DSC traces are reported in the SI.

**Thermogravimetric analysis (TGA).** TGA measurements were performed with a PerkinElmer TGA7 in the temperature range 30-300 ºC and 30-450 °C for urea, catechol and URCAT, respectively, under $N_2$ gas flow at a heating rate of 5 ºC $min^{-1}$.

**Single Crystal X-ray Diffraction.** Single Crystal data were collected at room temperature with an Oxford X´Calibur S CCD diffractometer equipped with a graphite monochromator (Mo-Kα radiation, λ = 0.71073 Å). Data collection and refinement details are listed in Table S1 (Supporting Information). The structure were solved with SHELXT-2014[43] and refined on full-matrix $F^2$ by means of SHELXL-2014[43] implemented in the Olex2 software.[44] All non-hydrogen atoms were refined anisotropically. Hydrogen atoms bound to nitrogen or oxygen atoms were either located from the Fourier map or added in calculated positions; $H_{CH}$ atoms were added in calculated position. All H atoms were refined riding on the corresponding C/N/O atoms. The software Mercury 3.10[45] was used to simulate powder patterns based on single crystal data. The program Schakal was used for graphical representations.[46] CCDC 1880413 contains the supplementary crystallographic data for this paper. These data are provided free of charge by The Cambridge Crystallographic Data Centre (CCDC).

**X-ray Diffraction from Powder.** X-Ray diffraction patterns were collected on a PANalytical X´Pert Pro Automated diffractometer equipped with an X´celerator detector in Bragg-Brentano geometry, using Cu-Kα radiation (λ = 1.5418 Å) without monochromator in the 3-50º 2θ range (step size 0.033º; time/step: 20 s; Soller slit 0,04 rad, antiscatter slit: ½, divergence slit: ¼ ; 40 mA*40kV).

**Urease inhibition experiments.** The inhibition of urease by URCAT was characterized at room temperature through pre-incubation experiments carried out by following a spectrophotometric assay in which cresol red was exploited as a colorimetric probe to monitor the overtime change in absorbance at 573 nm due to the increase of pH caused by urease activity.[42] A 100 µL solution of 30 nM urease from *Canavalia ensiformis* (jack bean) urease (JBU) dissolved in 50 mM HEPES buffer at pH 7.5, was diluted to 0.3 nM in 9.86 mL of 2 mM HEPES buffer at pH 7.50, also containing 2 mM EDTA and 30 mg $L^{-1}$ cresol red (CR solution). A 40-µL solution of 10 mM URCAT or catechol, dissolved in the same buffer, were added, taking the time when the enzyme solution and URCAT (or catechol) were mixed as zero time of incubation. After appropriate periods of time, 1-mL aliquots were withdrawn from the incubation solution, an 8 M solution of urea was added to a final concentration of 100 mM, and the change in absorbance over time was followed ($\lambda$= 573 nm). The activity was calculated by a linear fitting of the straight portion in the absorbance vs. time curve and normalized to the activity measured at time zero of incubation.

**Dynamic Vapor Sorption experiments.** The DVS Intrinsic (Surface Measurement Systems Ltd, USA), equipped with SMS Ultrabalance ™ having a mass resolution of ±0.1 µg, was used to obtain ramping and equilibrium water vapor sorption isotherms. An approximately 5 mg of powder samples were placed in the apparatus using aluminum pans and initially dried over 600 minutes with a stream of dry nitrogen to establish a dry mass at 25 °C. The dry mass was calculated after the end of first drying stage (0% RH). The sorption cycle experiments were performed from 0% relative humidity (RH) to 95% RH in a step of 5% RH in a preprogrammed sequence before decreasing to 0% RH in a reverse order. The instrument maintained a constant target RH until the moisture content change per minute (dm/dt) was less than 0.002% per minute over a 10-minute period.

The GAB analysis (Guggenheim-Anderson-DeBoer) isotherm,[47] with constants C and K, was converted to a second-order polynomial, giving a quadratic equation. The curve fitting parameters was evaluated using mean square error and mean relative percentage deviation.

The GAB model is given (1)

$$\frac{W}{W_m} = \frac{C_G * K * a_w}{(1 - K * a_w)[1 - K * a_w + C_G * K * a_w]} \quad (1)$$

where w is water content on a dry weight basis, $w_m$ is one molecule water per active sorption site, $a_w$ is water activity, $C_G$ is G.A.B sorption constant and K is a parameter in GAB equation. Most isotherm models in the literature, including BET and GAB, assume surface sorption only. For instance, BET and GAB describe monolayer water adsorption followed by multilayer water. These models are not able to accurately describe bulk, solution or absorbed water. Therefore, a GAB fitting procedure was applied here only to compare urea and URECAT qualitative differences upon water vapor adsorption.

## Results and Discussion

**The urea·catechol co-crystal structure**. The urea·catechol (URCAT) co-crystal of urea and catechol was prepared by milling of the two reactants in the 1:1 stoichiometric ratio (see the Experimental Section). Single crystals suitable for X-ray diffraction were grown from an ethanol solution of the reagents. Structural identity between the product of the solid-state synthesis and the product of the recrystallization via seeding was verified by comparing the XRPD pattern, calculated on the basis of the single crystal structure, and the experimental pattern measured for the crystalline powder (see Figure 1).

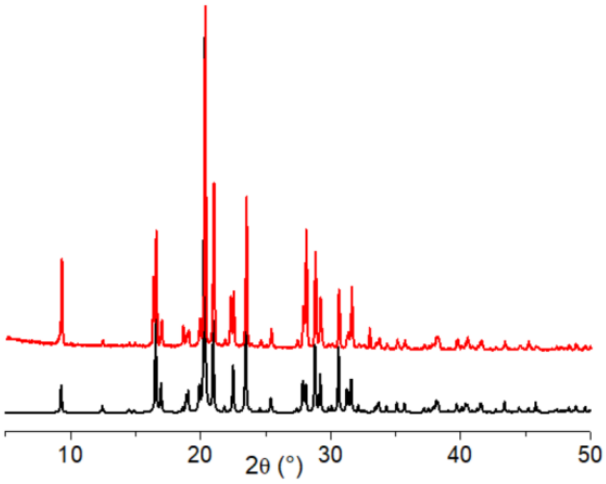


**Figure 1.** Comparison between the experimental patter (black line) measured of the product of the solid-state synthesis and the pattern (red line) calculated on the basis of the single crystal structure.

Figure 2 shows the main packing feature of crystalline URCAT: urea is organized in hydrogen bonded dimers, similarly to what observed in its pure crystal,[48] as shown in Figure 3a; all dimers are bridged by two catechol molecules, with the OH groups interacting via hydrogen bonds with the urea carbonyl groups [$O_{OH}\cdots O_{CO}$ 2.717(3) Å].

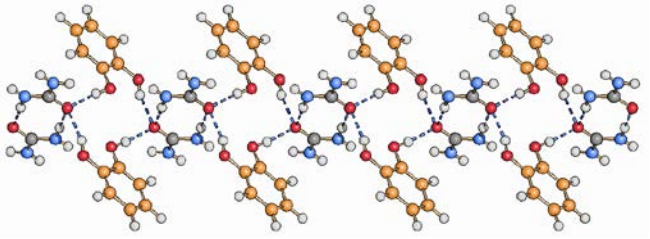

**Figure 2.** The main packing feature in crystalline URCAT: urea is organized in hydrogen-bonded dimers, which are bridged by catechol molecules, thus resulting in the formation of infinite ribbons. C (urea) atoms in grey, C (catechol) atoms in orange.

This results in the formation of infinite ribbons extending along the crystallographic *a*-axis. When comparing the crystal packing of the co-crystal with that of catechol[48] shown in Figure 3b, it can be seen that in pure catechol all molecules form hydrogen bonded dimers. In turn, each dimer interacts with four neighboring dimers arranged perpendicularly to the dimer plane. Therefore, the main difference arises from the fact that catechol in the co-crystal is hydrogen bonded only to urea; a similar pattern is present in the known catechol·2DMSO solvate[49] (refcode EPAVUN, Figure. 4): here hydrogen-bonded tetramers can be identified, formed by catechol molecules only, while the tetramers are bridged by the DMSO S=O groups, resulting in the formation of rings similar to those observed in crystalline URCAT (Figure. 2); all units are arranged in infinite ribbons extending along the crystallographic *c*-axis.

(a) (b)

**Figure 3**. Hydrogen-bonded dimers in crystalline urea (a) and catechol (b).

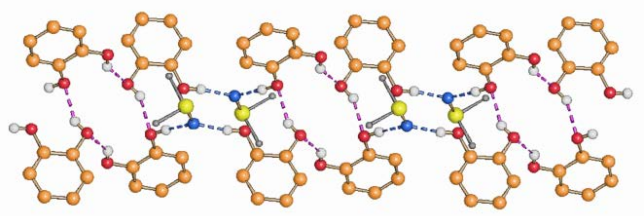

**Figure 4**. Hydrogen-bonded ribbon involving catechol and DMSO in the catechol·2DMSO solvate (EPAVUN). $H_{CH}$ atoms not shown for clarity; small grey spheres represent the methyl groups.

**Thermal stability of the co-crystal.** DSC measurements were performed using the urea-catechol co-crystal and the starting materials, i.e. urea and catechol, in the 40-150 °C range. No thermal events are present for the co-crystal before melting, which occurs at 76.4 °C (peak temperature). The co-crystal thus melts at a temperature that is definitely lower than those of its components, as can be seen from Figure 5. TGA measurements also show that, on heating, the co-crystal is stable up to ca. 80 °C, i.e. melting is almost immediately followed by decomposition.

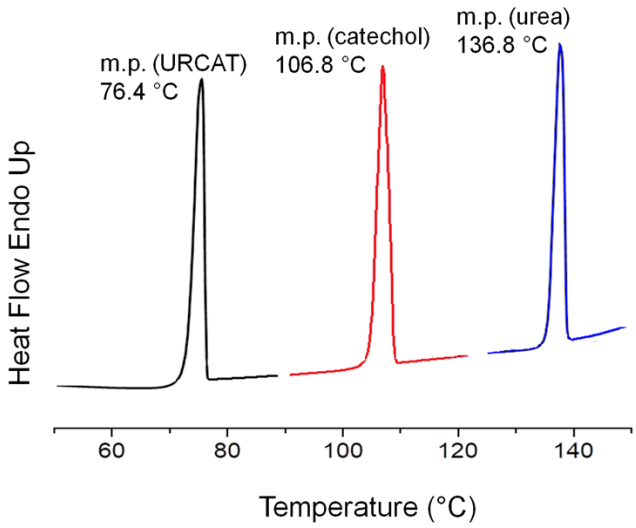


**Figure 5**. Comparison of the DSC traces for (from left to right) URCAT, catechol and urea.

**Urease inhibition experiments.** The inhibition of *Canavalia ensiformis* (jack bean) urease (JBU) by URCAT was studied by pre-incubating the enzyme with 40 µM inhibitor for increasing periods of time as previously described[41,42] and the residual activity was monitored using UV-Vis spectrophotometry. The inhibition of the enzyme by 40 µM catechol was also determined and used as a control and it is in complete agreement with previously published data.[42] The data in Figure 6 reporting the residual activity of urease as a function of pre-incubation time show a time-dependent inactivation process. In particular, a short initial lag phase is followed by an acceleration of the

inactivation course that yields a 50 % inactivation in ca. 5 mins leading to the eventual complete loss of urease activity in a 20-min period. The inactivation efficiency of URCAT on urease is largely comparable to that of catechol in the experimental conditions used, demonstrating that URCAT is a catechol-urea co-formulate efficient in controlling urease activity, *in vitro*.

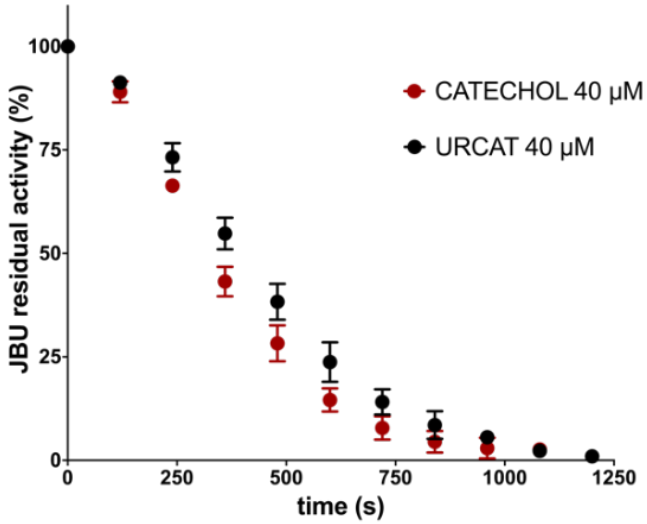


**Figure 6.** Residual JBU activity as a function of pre-incubation time of the enzyme in the presence of 40 µM URCAT (black dots) or 40 µM catechol (red dots). Data were measured as triplicates, mean and standard deviation (as bars) are reported.

**Dynamic Vapor Sorption (DVS) analysis.** The amount of the adsorbed water and urea and URCAT response to changes in relative humidity were investigated using constant temperature adsorption/desorption experiments by varying water as relative humidity. Results are shown in Figure 7. In particular, URCAT, when normalized per unit of surface area, $m^2$, adsorbs ~3.5 less water than urea at high RH. The relative humidity (RH) here is defined as where $P_o$ is the saturated vapor pressure of water at 298 K and 1 atm and $P$ is the actual water pressure at the same temperature and pressure, e.g.

$$RH = \frac{P}{P_o}\, x\, 100\ (\%) \qquad (2).$$

Additionally, both urea and URCAT DVS data exhibited hysteresis between the adsorption and desorption branches, albeit of different shapes. During the hydration of urea, water uptake remained negligible until deliquescence phase transition at 74 % RH, indicating sharp size increase and liquid layer formation on urea. Subsequently, with further increases in RH, the aqueous droplet underwent continuous hygroscopic growth. During the dehydration process, the representative urea particle showed a two-stage phase transition. The liquid droplet decreased gradually in size with decreasing RH and became supersaturated with respect to urea below RH of 74%. With further decrease in RH, effloresced particle was formed at RH of 50%. Notably, URCAT lacks a distinct efflorescence point as exhibited by a continuous hysteresis down to low (<20 % RH) values of a desorption branch. The direct absence of observable efflorescence point after deliquescence is reached suggests that some water remains bound in a structural form (H-bond or monolayer), especially at low RH. Further, water, still bound at intermediate RH (70 to 30 %), can be regarded as the continuous transition of the bound-to-free water with the vaporization enthalpy slightly higher than that for pure water.[50] It potentially indicates that strong hydrogen bonds were formed with URCAT hydrophilic and polar groups.

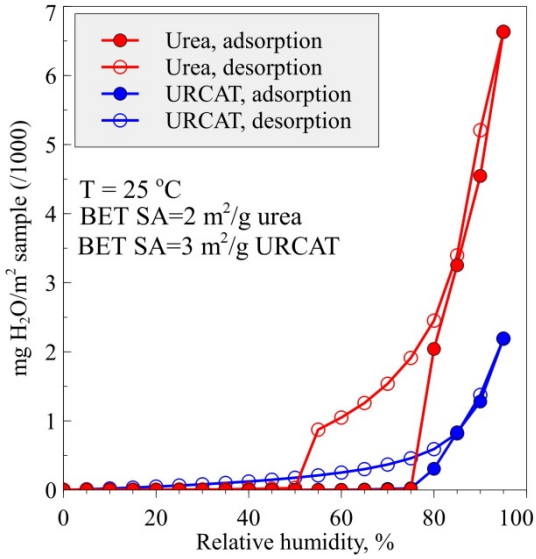


**Figure 7.** Adsorption/desorption branches of RH on urea and URCAT.

The water sorption (and retention) of URCAT was further elucidated using the GAB analysis (Guggenheim-Anderson-DeBoer) isotherm[47,51–53] as shown in Figure 8. The GAB model represents a refined extension of the BET theory postulating that the state of the sorbate molecules in the second and higher layers is equal, but different from that in the liquid-like state.[54] The fit parameters $m_o$ (the monolayer moisture content), C and K (constants related to the energies of interaction between the first and further molecules, e.g. monolayer and multilayer regions at the individual sorption sites), are related to the sorption enthalpies.

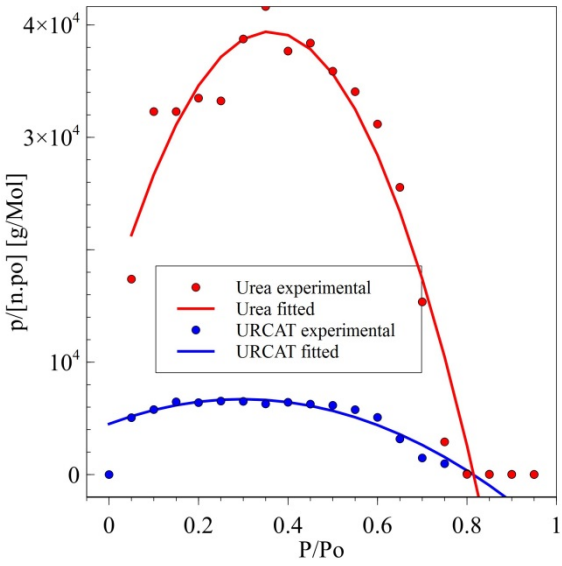


**Figure 8.** Resulting fits to the GAB model of urea and URCAT.

Accordingly, URCAT exhibited greater monolayer capacity (mol/g) than urea, as shown in Table 1. Further, the sorption constant C – describing a monolayer formation propensity - is greater for urea than for URCAT, while the multilayer region constant K is very similar for both samples. The higher monolayer capacity in URCAT can be related to its ability to retain water even at low humidity, as shown in Figure 7. Urea, on the other hand, shows stronger binding affinity towards monolayer water, as C can be directly related to the difference between the monolayer and multilayer molar sorption enthalpies.[55,56]

**Table 1.** Calculated RH absorption parameters obtained using GAB model

| Sample | $m_o$, monolayer capacity, mol/g | Sorption constant K | Sorption constant C |
|---|---|---|---|
| Urea | $5.73 \times 10^{-6}$ | 1.221 | 9.931 |
| URCAT | $3.59 \times 10^{-5}$ | 1.264 | 4.850 |

**Solubility test.** Solubility of urea at room temperature ranges from 1 to 1.2 g $mL^{-1}$, Therefore, a control experiment was conducted in which 1 g of urea was added to a vial and dissolved in 1 mL of bi-distilled water. In a second vial an amount of URCAT (2.8 g) containing 1 g of urea and 1 mL of bi-distilled water were then added: the dissolution was not complete after 5 minutes, as can be seen in Figure 9.

**Figure 9:** solubility test for URCAT in bidistilled water.

The undissolved solid was filtered and weighed, resulting in ca. 500 mg of powder material, which corresponds to a ca. 15% reduction of the solubility of urea in URCAT with respect to pure urea. The undissolved powder was analyzed via X-ray powder diffraction and found to be URCAT (Figure 10).

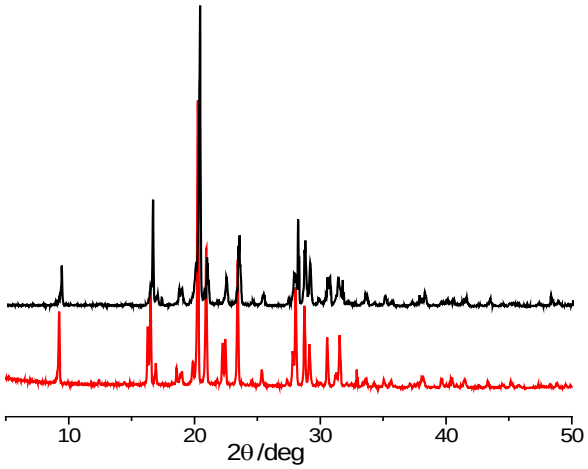


**Figure 10.** Experimental X-ray powder patterns for URCAT measured before the solubility test (red line) and on the residual powder after the solubility test (black line).

**Stability tests.** URCAT (2.8 g) and a physical mixture of urea (1 g) and catechol (1.8 g) were placed in two separate watch glasses inside a chamber at controlled humidity (82% RH) (see Figure 11, top). Degradation of catechol, visually observed after ca. 5 hours as a colour change from white to pinkish-brown (see Figure 11, bottom left), was confirmed via X-ray powder diffraction (see Figure 12); the URCAT co-crystal, on the contrary, did not show any modification after 5 hours, suggesting that the stability of catechol is markedly improved in URCAT with respect to pure catechol.

Physical mixture at t = 0 URCAT at t = 0

Physical mixture at t = 5h URCAT at t = 5h

**Figure 11.** Visual comparison of the physical mixture of urea and catechol (left) and the URCAT co-crystal (right) at t=0 (top) and after 5 hours at 82% RH (bottom).

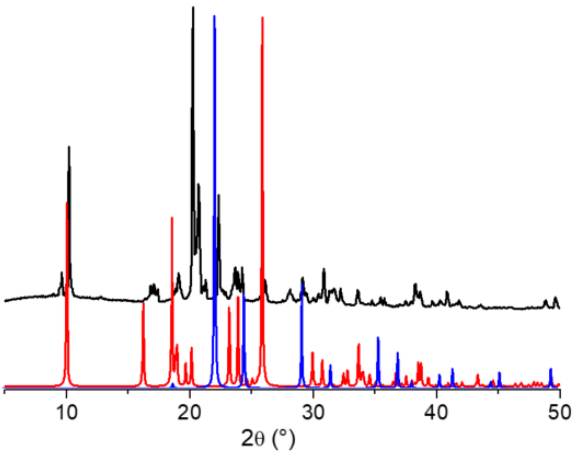


**Figure 12.** Comparison of the XRPD pattern measured on the physical mixture after 5 hours of exposition to 82% RH (black line), and the calculated patterns of the pure components (blue line for urea, red line for catechol).

**Conclusions and sustainability impact.**

A co-crystal of urea and catechol (URCAT) has successfully been synthesized by milling of the components. The resulting compound has been investigated thoroughly with a combination of solid state and biotechnological methods. Single crystals of URCAT have been grown from solution, and fully structurally characterized. The urea molecules within the co-crystal are organized in hydrogen bonded dimers bridged by two catechol molecules, with the OH groups interacting via hydrogen bonds with the urea carbonyl groups. The co-crystal exhibits a melting temperature of 76.4 $^{o}$C, lower than that of pure reactants. The inhibition of jack bean urease enzyme by URCAT leads to the complete loss of urease activity after a 20-min incubation period. These data are comparable to that of catechol itself, demonstrating that URCAT is a catechol-urea co-formulate efficient in controlling urease activity, *in vitro*. Stability of URCAT as compared to urea in the presence of $H_2O$ vapor was inferred using dynamic vapor sorption experiments. A large difference of water vapor adsorption was observed between urea and URCAT, with the latter adsorbing 3.5 times less water than urea. A higher propensity of URCAT to retain adsorbed water at low relative humidity as compared to urea was also observed.

In conclusion, while inhibition of urease activity with the previously investigated urea·$ZnCl_2$·KCl co-crystal was achieved via inorganic salts complexation,[28] the co-crystallization of urea and catechol affords an organic-only material that can act both as soil fertilizer and efficacious urease inhibitor. Our results lend further support to the idea that co-crystal engineering strategies[57] can be successfully applied to tackle agricultural, food production, and environmental issues. In particular, the food, energy, and water systems are delicately linked in conventional agricultural production, especially with respect to fertilizer systems. As world's population and the corresponding food production continues to grow, meeting the fertilizer demands for crops will

become more difficult and add increasing pressure on our water and energy systems. This is partially due to the nitrogen losses associated with the little environmental stability of urea under humid conditions. Our results show that URCAT can serve not only as an inhibitor to minimize urea nitrogen losses but it also possesses improved environmental stability. Utilizing such urea co-crystals has the ability to decrease a significant portion of fertilizer demand while potentially enhancing this food-energy-water system sustainability. If effective in the field, it may help lower ammonia emissions, increase nitrogen use efficiency by using less product (smaller environmental footprint) to maintain crop yields for a growing population. Finally, if effective in the field, it may help lower the amount of nitrate leaching. This would allow plants more of an opportunity to uptake nitrate before the nitrate is leached beneath the rooting zone.

**Acknowledgements**

This material is based upon K.H and J.B. work supported by the National Science Foundation under Grant Number CHE-1710120 and upon D.B., F.G., L.M. and S.L.C. work supported by the University of Bologna (RFO scheme).

**Supporting Information.** TGA, DSC, crystal data and details of measurement for URCAT are supplied as Supporting Information.

## References


(1) Agriculture and Production & International Trade services. Fertilizer Outlook 2017–2021. In *International Fertilizer Association (IFA) Annual Conference*; Marrakech (Marocco)., 2017.

(2) Zhu, X.; Burger, M.; Doane, T. A.; Horwath, W. R. Ammonia Oxidation Pathways and Nitrifier Denitrification Are Significant Sources of N(2)O and NO under Low Oxygen Availability. *Proc. Natl. Acad. Sci. U. S. A.* **2013**, *110* (16), 6328–6333. https://doi.org/10.1073/pnas.1219993110.

(3) Hewitt, C. N.; MacKenzie, A. R.; Di Carlo, P.; Di Marco, C. F.; Dorsey, J. R.; Evans, M.; Fowler, D.; Gallagher, M. W.; Hopkins, J. R.; Jones, C. E.; Langford B.; Lee J.D.; Lewis A.C.; Lim S.F.; McQuaid J.; Misztal P.; Moller S.J.; Monks P.S.; Nemitz E.; Oram D.E.; Owen S.M.; Phillips G.J.; Pugh T.A.; Pyle J.A.; Reeves C.E.; Ryder J.; Siong J.; Skiba U.; Stewart D.J. Nitrogen Management Is Essential to Prevent Tropical Oil Palm Plantations from Causing Ground-Level Ozone Pollution. *Proc. Natl. Acad. Sci.* **2009**, *106* (44), 18447 LP-18451. https://doi.org/10.1073/pnas.0907541106

(4) Oikawa, P. Y.; Ge, C.; Wang, J.; Eberwein, J. R.; Liang, L. L.; Allsman, L. A.; Grantz, D. A.; Jenerette, G. D. Unusually High Soil Nitrogen Oxide Emissions Influence Air Quality in a High-Temperature Agricultural Region. *Nat. Commun.* **2015**, *6*, 8753. https://doi.org/10.1038/ncomms9753

(5) Diaz, R. J.; Rosenberg, R. Spreading Dead Zones and Consequences for Marine Ecosystems. *Science (80-. ).* **2008**, *321* (5891), 926–929. DOI: 10.1126/science.1156401

(6) Duce, R. A.; LaRoche, J.; Altieri, K.; Arrigo, K. R.; Baker, A. R.; Capone, D. G.; Cornell,

S.; Dentener, F.; Galloway, J.; Ganeshram, R. S.; Geider R.J.; Jickells T.; Kuypers M.M.; Langlois R.; Liss P.S.; Liu S.M.; Middelburg J.J.; Moore C.M.; Nickovic S.; Oschlies A.; Pedersen T.; Prospero J.;, Schlitzer R.; Seitzinger S.; Sorensen L.L.; Uematsu M.; Ulloa O.; Voss M.; Ward B.; Zamora L. Impacts of Atmospheric Anthropogenic Nitrogen on the Open Ocean. *Science (80-. ).* **2008**, *320* (5878), 893–897. DOI: 10.1126/science.1150369

(7) Galloway, J. N.; Cowling, E. B. Reactive Nitrogen and the World: 200 Years of Change. *Ambio* **2002**, *31* (2), 64—71. https://doi.org/10.1579/0044-7447-31.2.64.

(8) Galloway, J. N.; Aber, J. D.; Erisman, J. W.; Seitzinger, S. P.; Howarth, R. W.; Cowling, E. B.; Cosby, B. J. The Nitrogen Cascade. *Bioscience* **2003**, *53* (4), 341–356. https://doi.org/10.1641/0006-3568(2003)053[0341:TNC]2.0.CO;2

(9) Galloway, J. N.; Dentener, F. J.; Capone, D. G.; Boyer, E. W.; Howarth, R. W.; Seitzinger, S. P.; Asner, G. P.; Cleveland, C. C.; Green, P. A.; Holland, E. A.; Karl D. M.; Michaels A. F.; Porter J. H.; Townsend A. R.; Vörösmarty C. J. Nitrogen Cycles: Past, Present, and Future. *Biogeochemistry* **2004**, *70* (2), 153–226. https://doi.org/10.1007/s10533-004-0370-0.

(10) Kiss, S.; Simihaian, M. *Improving Efficiency of Urea Fertilizers by Inhibition of Soil Urease Activity*; Springer Netherlands, 2002. https://doi.org/10.1007/978-94-017-1843-1.

(11) Zhang, X.; Davidson, E. A.; Mauzerall, D. L.; Searchinger, T. D.; Dumas, P.; Shen, Y. Managing Nitrogen for Sustainable Development. *Nature* **2015**, *528*, 51-59. https://doi.org/10.1038/nature15743

(12) Rockström, J.; Steffen, W.; Noone, K.; Persson, Å.; Chapin III, F. S.; Lambin, E. F.; Lenton, T. M.; Scheffer, M.; Folke, C.; Schellnhuber, H. J.; Nykvist B.; de Wit C.Aa.;

Hughes T.; van der Leeuw S.; Rodhe H.; Sörlin S.; Snyder P.K.; Costanza R.; Svedin U.; Falkenmark M.; Karlberg L.; Corell R.W.; Fabry V.J.; Hansen J.; Walker B.; Liverman D.; Richardson K.; Crutzen P.; Foley J.A. A Safe Operating Space for Humanity. *Nature* **2009**, *461*, 472-475. https://doi.org/10.1038/461472a

(13) Coskun, D.; Britto, D. T.; Shi, W.; Kronzucker, H. J. Nitrogen Transformations in Modern Agriculture and the Role of Biological Nitrification Inhibition. *Nat. Plants* **2017**, *3*, 17074. https://doi.org/10.1038/nplants.2017.74

(14) Bremner, J. M.; Douglas, L. A. Inhibition of Urease Activity in Soils. *Soil Biol. Biochem.* **1971**, *3* (4), 297–307. https://doi.org/10.1016/0038-0717(71)90039-3.

(15) Krupa, S. V. Effects of Atmospheric Ammonia (NH3) on Terrestrial Vegetation: A Review. *Environ. Pollut.* **2003**, *124* (2), 179–221. https://doi.org/10.1016/S0269-7491(02)00434-7.

(16) Hand, J. L.; Schichtel, B. A.; Pitchford, M.; Malm, W. C.; Frank, N. H. Seasonal Composition of Remote and Urban Fine Particulate Matter in the United States. *J. Geophys. Res. Atmos.* **2012**, *117* (D5). https://doi.org/10.1029/2011JD017122.

(17) Pope, C. A.; Ezzati, M.; Dockery, D. W. Fine-Particulate Air Pollution and Life Expectancy in the United States. *N. Engl. J. Med.* **2009**, *360* (4), 376–386. https://doi.org/10.1056/NEJMsa0805646.

(18) Paulot, F.; Jacob, D. J. Hidden Cost of U.S. Agricultural Exports: Particulate Matter from Ammonia Emissions. *Environ. Sci. Technol.* **2014**, *48* (2), 903–908. https://doi.org/10.1021/es4034793.

(19) Kafarski, P.; Talma, M. Recent Advances in Design of New Urease Inhibitors: A Review. *J. Adv. Res.* **2018**, *13*, 101–112. https://doi.org/10.1016/j.jare.2018.01.007.

(20) Zambelli, B.; Musiani, F.; Benini, S.; Ciurli, S. Chemistry of Ni2+ in Urease: Sensing, Trafficking, and Catalysis. *Acc. Chem. Res.* **2011**, *44* (7), 520–530. https://doi.org/10.1021/ar200041k.

(21) Mazzei, L.; Musiani, F.; Ciurli, S. CHAPTER 5 Urease. In *The Biological Chemistry of Nickel*; The Royal Society of Chemistry, 2017; pp 60–97. https://doi.org/10.1039/9781788010580-00060.

(22) Maroney, M. J.; Ciurli, S. Nonredox Nickel Enzymes. *Chem. Rev.* **2014**, *114* (8), 4206–4228. https://doi.org/10.1021/cr4004488.

(23) Mazzei, L.; Cianci, M.; Contaldo, U.; Musiani, F.; Ciurli, S. Urease Inhibition in the Presence of N-(n-Butyl)Thiophosphoric Triamide, a Suicide Substrate: Structure and Kinetics. *Biochemistry* **2017**, *56* (40), 5391–5404. https://doi.org/10.1021/acs.biochem.7b00750.

(24) Krogmeier, M. J.; McCarty, G. W.; Bremner, J. M. Potential Phytotoxicity Associated with the Use of Soil Urease Inhibitors. *Proc. Natl. Acad. Sci. U. S. A.* **1989**, *86* (4), 1110–1112. https://doi.org/10.1073/pnas.86.4.1110

(25) Zanin, L.; Tomasi, N.; Zamboni, A.; Varanini, Z.; Pinton, R. The Urease Inhibitor NBPT Negatively Affects DUR3-Mediated Uptake and Assimilation of Urea in Maize Roots . *Frontiers in Plant Science* . 2015, p 1007. https://doi.org/10.3389/fpls.2015.01007

(26) Tarsia, C.; Danielli, A.; Florini, F.; Cinelli, P.; Ciurli, S.; Zambelli, B. Targeting

Helicobacter Pylori Urease Activity and Maturation: In-Cell High-Throughput Approach for Drug Discovery. *Biochim. Biophys. Acta - Gen. Subj.* **2018**, *1862* (10), 2245–2253. https://doi.org/10.1016/j.bbagen.2018.07.020.

(27) Mazzei, L.; Broll, V.; Ciurli, S. An Evaluation of Maleic-Itaconic Copolymers as Urease Inhibitors. *Soil Sci. Soc. Am. J.* **2018**, *82*, 994–1003. https://doi.org/10.2136/sssaj2017.09.0323.

(28) Casali, L.; Mazzei, L.; Shemchuk, O.; Honer, K.; Grepioni, F.; Ciurli, S.; Braga, D.; Baltrusaitis, J. Smart Urea Ionic Co-Crystals with Enhanced Urease Inhibition Activity for Improved Nitrogen Cycle Management. *Chem. Commun.* **2018**, *54* (55), 7637–7640. https://doi.org/10.1039/C8CC03777A.

(29) Sandhu, B.; Sinha, A. S.; Desper, J.; Aakeröy, C. B. Modulating the Physical Properties of Solid Forms of Urea Using Co-Crystallization Technology. *Chem. Commun.* **2018**, *54* (37), 4657–4660. https://doi.org/10.1039/C8CC01144C.

(30) Honer, K.; Kalfaoglu, E.; Pico, C.; McCann, J.; Baltrusaitis, J. Mechanosynthesis of Magnesium and Calcium Salt–Urea Ionic Cocrystal Fertilizer Materials for Improved Nitrogen Management. *ACS Sustain. Chem. Eng.* **2017**, *5* (10), 8546–8550. https://doi.org/10.1021/acssuschemeng.7b02621.

(31) Honer, K.; Pico, C.; Baltrusaitis, J. Reactive Mechanosynthesis of Urea Ionic Cocrystal Fertilizer Materials from Abundant Low Solubility Magnesium- and Calcium-Containing Minerals. *ACS Sustain. Chem. Eng.* **2018**, *6* (4), 4680–4687. https://doi.org/10.1021/acssuschemeng.7b03766.

(32) Theophanides, T.; Harvey, P. D. Structural and Spectroscopic Properties of Metal-Urea

Complexes. *Coord. Chem. Rev.* **1987**, *76*, 237–264. https://doi.org/https://doi.org/10.1016/0010-8545(87)85005-1.

(33) Smith, G.; Baldry, K. E.; Byriel, K. A.; Kennard, C. H. L. Molecular Cocrystals of Carboxylic Acids. XXV The Utility of Urea in Structure Making with Carboxylic Acids and the Crystal Structures of a Set of Six Adducts with Aromatic Acids. *Aust. J. Chem.* **1997**, *50* (7), 727–736.

(34) Hargittai, M. H. I. NOVEL INCLUSION COMPOUNDS WITH UREA/THIOUREA/SELENOUREA ANION HOST LATTICES. In *Advances in Molecular Structure Research*; Jai Press, 1998; pp 151–225. DOI: 10.1007/BF02900545

(35) Huang, L.; Tonelli, A. E. Inclusion Compounds as a Means to Fabricate Controlled Release Materials. In *Intelligent Materials for Controlled Release*; ACS Symposium Series; American Chemical Society, 1999; Vol. 728, pp 10–131. https://doi.org/doi:10.1021/bk-1999-0728.ch010.

(36) Purakayastha, T. J.; Katyal, J. C. Evaluation of Compacted Urea Fertilizers Prepared with Acid and Non-Acid Producing Chemical Additives in Three Soils Varying in PH and Cation Exchange Capacity; I. NH3 Volatilization. *Nutr. Cycl. Agroecosystems* **1998**, *51* (2), 107–115. https://doi.org/10.1023/A:1009785420209.

(37) Moawad, H.; Enany, M. H.; Badr El-Din, S. M. S.; Mahmoud, S. A. Z.; Gamal, R. F. Transformations and Effects of Urea Derivatives in Soil. *Zeitschrift für Pflanzenernährung und Bodenkd.* **1984**, *147* (6), 785–792. https://doi.org/10.1002/jpln.19841470617.

(38) Von Rheinbaben, W. Effect of Magnesium Sulphate Addition to Urea on Nitrogen Loss

Due to Ammonia Volatilization. *Fertil. Res.* **1987**, *11* (2), 149–159. https://doi.org/10.1007/BF01051058.

(39) Fenn, L. B.; Richards, J. Ammonia Loss from Surface Applied Urea-Acid Products. *Fertil. Res.* **1986**, *9* (3), 265–275. https://doi.org/10.1007/BF01050352.

(40) Fenn, L. B.; Hossner, L. R. Ammonia Volatilization from Ammonium or Ammonium-Forming Nitrogen Fertilizers BT - Advances in Soil Science; Stewart, B. A., Ed.; Springer New York: New York, NY, 1985; pp 123–169. https://doi.org/10.1007/978-1-4612-5046-3_4.

(41) Mazzei, L.; Cianci, M.; Musiani, F.; Ciurli, S. Inactivation of Urease by 1,4-Benzoquinone: Chemistry at the Protein Surface. *Dalt. Trans.* **2016**, *45* (13), 5455–5459. https://doi.org/10.1039/C6DT00652C.

(42) Mazzei, L.; Cianci, M.; Musiani, F.; Lente, G.; Palombo, M.; Ciurli, S. Inactivation of Urease by Catechol: Kinetics and Structure. *J. Inorg. Biochem.* **2017**, *166*, 182–189. https://doi.org/10.1016/j.jinorgbio.2016.11.016.

(43) Sheldrick, G. M. SHELXT - Integrated Space-Group and Crystal-Structure Determination. *Acta Crystallogr. Sect. A Found. Adv.* **2015**, *A71*, 3–8. https://doi.org/10.1107/S2053273314026370.

(44) Dolomanov, O. V; Bourhis, L. J.; Gildea, R. J.; Howard, J. A. K.; Puschmann, H. OLEX2: A Complete Structure Solution, Refinement and Analysis Program. *J. Appl. Crystallogr.* **2009**, *42* (2), 339–341. https://doi.org/10.1107/S0021889808042726.

(45) Macrae, C. F.; Edgington, P. R.; McCabe, P.; Pidcock, E.; Shields, G. P.; Taylor, R.;

Towler, M.; van de Streek, J. Mercury: Visualization and Analysis of Crystal Structures. *J. Appl. Crystallogr.* **2006**, *39* (3), 453–457. https://doi.org/10.1107/S002188980600731X.

(46) Keller, E. Neues von SCHAKAL. *Chemie unserer Zeit* **1986**, *20* (6), 178–181. https://doi.org/10.1002/ciuz.19860200603.

(47) van den Berg, C. Development of B.E.T.-Like Models for Sorption of Water on Foods, Theory and Relevance BT - Properties of Water in Foods: In Relation to Quality and Stability. In *Properties of Water in Foods in Relation to Quality and Stability*; Simatos, D., Multon, J. L., Eds.; Springer Netherlands: Dordrecht, 1985; pp 119–131. https://doi.org/10.1007/978-94-009-5103-7_8.

(48) Brown, C. J. The Crystal Structure of Catechol. *Acta Crystallogr.* **1965**, *21* (1), 170–174. https://doi.org/10.1107/S0365110X66002482.

(49) Polyanskaya, T. M.; Khaldoyanidi, K. A.; Smolentsev, A. I. Supramolecular Architecture of Catechol and Its 2:1 Complex with Dimethylsulfoxide. *J. Struct. Chem.* **2010**, *51* (2), 327–334. https://doi.org/10.1007/s10947-010-0050-y.

(50) Basu, S.; Shivhare, U. S.; Mujumdar, A. S. Models for Sorption Isotherms for Foods: A Review. *Dry. Technol.* **2006**, *24* (8), 917–930. https://doi.org/10.1080/07373930600775979.

(51) Guggenheim, E. A. *Applications of Statistical Mechanics*; Oxford University Press, 1966.

(52) Anderson, R. B. Modifications of the Brunauer, Emmett and Teller Equation. *J. Am. Chem. Soc.* **1946**, *68* (4), 686–691. https://doi.org/10.1021/ja01208a049.

(53) Boer, J. H. *The Dynamical Character of Adsorption*; Clarendon Press, Oxford U.K, 1953.

(54) Al-Muhtaseb, A. H.; McMinn, W. A. M.; Magee, T. R. A. Moisture Sorption Isotherm Characteristics of Food Products: A Review. *Food Bioprod. Process.* **2002**, *80* (2), 118–128. https://doi.org/10.1205/09603080252938753.

(55) van den Berg, C.; Bruin, S. Water Activity and Its Estimation in Food Systems: Theoretical Aspects. In *Water Activity: Influences on Food Quality*; Rockland, L. B., Stewart, G., Eds.; Academic Press, 1981; pp 1–61. https://doi.org/10.1016/B978-0-12-591350-8.50007-3.

(56) Kapsalis, J. G. MOISTURE SORPTION HYSTERESIS. In *Water Activity: Influences on Food Quality*; Rockland, L. B., Stewart, G., Eds.; Academic Press, 1981; pp 143–177. https://doi.org/10.1016/B978-0-12-591350-8.50011-5.

(57) Braga, D.; Grepioni, F.; Shemchuk, O. Organic–inorganic Ionic Co-Crystals: A New Class of Multipurpose Compounds. *CrystEngComm* **2018**, *20* (16), 2212–2220. https://doi.org/10.1039/C8CE00304A.

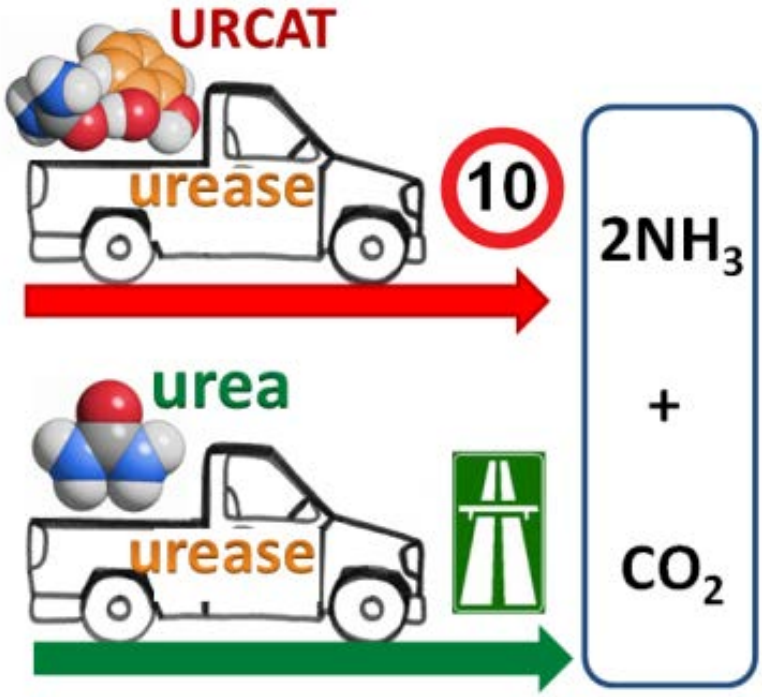


TOC. **Dual-action urea co-crystal:** Mechanochemical co-crystallization of urea and catechol affords an organic-only material that can act both as soil fertilizer and efficacious urease inhibitor. The novel compound has been characterized using solid state methods, and its environmental activity has been assessed using inhibition of *Canavalia ensiformis* urease and water vapor sorption experiments.